Network Identification Using μ-PMU and Smart Meter Measurements

Priyank Shah, *Student Member, IEEE* and Xiaowei Zhao

***Abstract*- The network identification plays a very prominent role for the network operator to accomplish the various objectives such as state-estimation, monitoring, control, planning, and real-time analytics. The network structure varies from time-to-time and its details are often not available with the network operator. To address this issue, an alternating direction method of multipliers (ADMM) based framework is presented herein to identify the network topology and line parameters using smart meter (SM) and micro phasor measurement unit (μ-PMU) measurements. The presented algorithm is divided into two sections, 1) approximate parameter evaluation through regression, to extract the partial topology information, and 2) complete network topology identification through the ADMM framework. This algorithm accomplishes the objectives of identifying the network configuration, branch parameters (e.g., conductance and susceptance), and change in branch parameters. Simulation results demonstrate the effectiveness of the presented algorithm on the benchmarked IEEE 13-bus and IEEE 123-bus feeders under various operating scenarios. Furthermore, the presented framework illustrates excellent network identification even with the presence of the stochastic nature of renewable power generation. The presented algorithm exhibits an excellent performance even with the consideration of noise in both measurements. In addition, the comparative performance is carried out on the benchmarked unbalanced IEEE 13-bus and balanced IEEE 33-bus feeders to highlight the efficacy of the presented framework over the state-of-art framework.**

***Keywords*- Grid parameter estimation, Distribution feeder, Phasor measurement unit (PMU), Smart grid, and Smart meter.**

I. INTRODUCTION

Nowadays, the phasor measurement units (PMUs) are widely popular in the electrical grid in order to acquire system information (e.g. magnitude and phase). This traditional PMU has good estimation accuracy for the long transmission line as the network has a significant phase difference between the buses, however, it is not the same in the case of the low-voltage distribution feeders [1]. Hence, the researchers have introduced a micro-phasor measurement unit (μ-PMU) device to improve the estimation accuracy for a low-voltage distribution network. In addition, the smart meter (SM) device is also popular in the network to acquire active power, reactive power, and voltage magnitude measurements. The measurements from the SMs and μ-PMUs are very helpful for a network operator to achieve the optimal operation [2-3] of the distribution network.

The network identification helps the network operator to accomplish the operations [4-5] such as state estimation, network expansion, network planning, fault detection, etc. It is well-known fact that the state-estimation algorithm is successful only when the system topology and the line parameters of the system are accurately known. Therefore, various algorithms are reported in the literature [6-8] to identify the network structure accurately, with the synchronized voltage and current samples. The machine-learning algorithm [8] needs enough time to let the algorithm learn and develops enough to comply their purpose with a considerable amount of accuracy and relevancy. This algorithm [8] is autonomous but highly susceptible to errors and it may not be able to discover immediately. These graphical algorithms [6-8] are not able to identify the line parameters, change in branch parameters, etc. In contrast with the graphical algorithm [6-8], the maximum likelihood estimation method is analyzed in [9] to estimate the branch parameters and network configuration using μ-PMU data. Although this method provides robust operation with the presence of noise, it fails to suffice identification objectives for an unbalanced distribution network. To overcome these shortcomings, the least absolute shrinkage and selection operator (Lasso) algorithm is analyzed in the literature [10-11] to identify the line parameters, event, change in structure for low-voltage feeders. Nevertheless, there are several scenarios in the low-voltage feeders where synchronized data (e.g., voltage, current) are not available to study due to having the high cost of a μ-PMU device, which creates a hindrance to accomplishing the identification objectives. Hence, the smart meter is an emerging device in low-voltage feeders to acquire system information.

The affinity propagation clustering-based approach is reported in [12] for the connectivity identification in a low-voltage distribution feeder using smart meter data. Although these algorithms [12-13] identify the network configuration, they are not capable to identify the network branch parameters with the presence of Gaussian noise in the measurements. The topology identification algorithm [13] is formulated using the weighted least square framework via multiagent systems. This framework [13] does not comply with the identification objectives such as branch parameters, changes in network configuration, etc. Peppanen *et al.* [14] have constructed the series-circuit regression model for network identification using SM data. Howbeit, this series-circuit model is less accurate and possibly invokes mistakes while performing the pairing process. Likewise, it fails to facilitate the new upstream node into the existing model, which may render erroneous results. To overcome these shortfalls, Shi *et al.* [15] have described the parallel-circuit regression model to identify the network configuration. Nonetheless, this algorithm [15] may not suffice the identification objectives with the presence of noise in smart meter data for unbalanced distributed systems.

To overcome these shortcomings, the mixed-integer linear/quadratic programming (MILP/MIQP) based algorithm is developed in [16] to identify the network configuration and outages for the unbalanced distribution network. However, it suffers from high-dimensionality issues and a high computational burden. Zhang *et al.* [17] have developed a numerical approach to identify the branch parameters, topology, and sudden change in the network using SM data. The Markov random filed technique is analyzed in [18] to accomplish the topology identification for the distribution network. This algorithm lacks to solve long-distance correlations of observation sequences and is

P. Shah and X. Zhao are with the Intelligent Control and Smart Energy (ICSE) research group, School of Engineering, The University of Warwick, Coventry, CV4 7AL, United Kingdom. (e-mails: {Priyank.shah, Xiaowei.zhao}@warwick.ac.uk).

This work was funded by the UK Engineering and Physical Sciences Research Council (EPSRC) under grant EP/S001905/1.

TABLE-I COMPARISONS BETWEEN EXISTING FRAMEWORKS

References	Type of Network	Topology Identification	Event Detection	Parameter Estimation
Prostejovsky *et al.* [2]	Balanced	Not Feasible	Not Feasible	Feasible
	Unbalanced	Not Feasible	Not Feasible	Not Feasible
Babakmehr *et al.* [4]	Balanced	Feasible	Feasible	Feasible
	Unbalanced	Not Feasible	Not Feasible	Not Feasible
Hosseini *et al.* [8]	Balanced	Feasible*	Not Feasible	Not Feasible
	Unbalanced	Feasible*	Not Feasible	Not Feasible
Si *et al* [12]	Balanced	Feasible	Feasible	Not Feasible
	Unbalanced	Not Feasible	Not Feasible	Not Feasible
Gandluru *et al.* [16]	Balanced	Feasible	Feasible	Not Feasible
	Unbalanced	Feasible	Feasible	Not Feasible
Zhang *et al.* [17]	Balanced	Feasible	Feasible	Feasible
	Unbalanced	Not Feasible	Not Feasible	Not Feasible
He *et al.* [21]	Balanced	Feasible	Feasible	Not Feasible
	Unbalanced	Not Feasible	Not Feasible	Not Feasible
Tian *et al.* [22]	Balanced	Feasible	Feasible	Not Feasible
	Unbalanced	Not Feasible	Not Feasible	Not Feasible

*It performs only phase identification for a balanced and unbalanced network.

susceptible to obtaining accurate local optimal solutions. In addition, it overlooks to analyze the impact of the stochastic nature of renewable power generation on network identification objectives. The impact of a renewable energy sources is studied on the benchmarked network configuration [19-21]. Papadopoulos et al. [19] have developed a probabilistic framework to study the dynamics and impact of uncertainties associated with the variation in network configuration, events, and stochastic nature of renewable energy sources. Nevertheless, the overall analysis depends upon the accurate availability of the network configuration and event location. To deal with these issues, the auto-regression model and random matrix theory-based hybrid framework is described in [21] to identify the network configuration and event detection for the given network. Nonetheless, the state-of-art framework [21] does not capable to estimate the branch parameters for either balanced or unbalanced system configuration. The comparative summary between various frameworks to identify the network configuration, event, and branch parameters is summarized in Table-I. Therefore, it is necessary to formulate a robust algorithm to accomplish the identification objectives with help of synchronized (e.g., μ-PMU) and non-synchronized (e.g., smart meter) data.

In this paper, a robust alternating direction method of multipliers (ADMM) is presented, to identify the network structure, branch parameters, event detection, etc., using μ-PMU and SM measurements. The salient features of the presented work are summarized as follows.

- The presented ADMM based algorithm leverages the measurements from both SMs and μ-PMUs, for accurate network identification, whereas, the state-of-art algorithms [10, 17, 22] deals with uniform measurements (e.g., either μ-PMUs or smart meters) to fulfil the identification objectives.
- The presented framework provides robust and efficacious identification performance even with wide variations of standard deviation in the μ-PMUs and smart meters measurements. In addition, the scalability and efficacy of the presented framework are validated through the benchmarked IEEE 123-bus feeder.
- The presented framework accomplishes the network identification objectives even with the presence of the stochastic nature of renewable power generation. To validate this feature, the performance is validated on benchmarked IEEE 13-bus feeders with the presence of renewable energy sources on certain buses.
- As the presented framework does not depend upon the types of loads, it accomplishes the network identification objectives without having particular knowledge of the number of households and its load profile.
- In contrast with the state-of-art methods [4, 6, 17, 22], the presented algorithm efficiently estimates the network configuration, branch parameters, change in branch parameters, and change or event in network structure. It is validated for an unbalanced IEEE 13-bus network with the opening of a three-phase branch (e.g. branch 671-692) and connection of a three-phase branch (e.g., branch between 680 to 692).
- Illustrative comparative performances are carried out to validate the effectiveness of the presented algorithm over traditional algorithms [10-11, 17]. The comparative identification result is demonstrated to estimate the revised branch parameters with the 10% variation in branch parameters (e.g., branch between 671 to 680) on the IEEE 13-bus unbalanced feeder. In addition, the comparative estimation of branch parameters is analyzed between the presented and state-of-art framework [17] on the benchmarked IEEE 33-bus balanced feeder with the presence of Gaussian noise.

The methodology for network identification is described in Section-II. In Section-III, the results and discussion for the presented framework are analyzed for the modified IEEE 13-bus and IEEE 132-bus feeders under various operating scenarios such as a change in branch parameter, change in network structure. To demonstrate the effectiveness of the presented framework over the traditional frameworks [10-11, 17], the comparative performances are analyzed in Section-IV. The conclusions are described in Section-V.

II. METHODOLOGY FOR NETWORK IDENTIFICATION

The methodology for network identification is reported in this section. Initially, the available measurements are described, obtained from the smart meters and μ-PMUs installed at various nodes in the network. Later, a method to obtain the partial information of the topology using only the smart meter measurements is described. Finally, the μ-PMU measurements are used to obtain the complete network identification. The topology information, as well as the conductances and susceptances of each of the lines, is obtained through this method. The methodology is thus organized in three subsections, described as follows.

A. Available Measurements

The measurements are available from the smart meters and the distributed phasor measurement units. The measurements available from the smart meters are the real and reactive

power injections and the voltage magnitudes, while the measurements with distributed phasor measurement units include the time-stamped voltage phasors and the current phasors. It is assumed that the smart meters are installed at certain buses, while the phasor measurement units are installed at the rest of the buses. Assuming that 'G_{ij}' and 'B_{ij}' are the susceptance and conductance of a line between the nodes 'i' and 'j' ($i, j \in \mathbb{N}$), then the active and reactive power injections at a given bus can be written as [23],

$$P_i = |V_i| \sum_{j=1}^{n} |V_j| \left(G_{ij} \cos\theta_{ij} + B_{ij} \sin\theta_{ij}\right) \quad (1)$$

$$Q_i = |V_i| \sum_{j=1}^{n} |V_j| \left(G_{ij} \sin\theta_{ij} - B_{ij} \cos\theta_{ij}\right) \quad (2)$$

where 'P_i' and 'Q_i' are the nodal real power and reactive power injections, while $|V_i|$ represents the voltage magnitude at a node 'i'. The smart meter measurements are initially processed using (1)-(2) as base equations, in order to extract the partial information of the topology, while the μ-PMU measurements are then utilized to extract the complete topology information.

B. Extraction of Partial Topology Information using Smart Meter Measurements

Assuming that the smart meter measurements are available only at certain nodes, the partial information about the network topology is extracted using the corresponding measurements. This information is extracted in two main steps. The first step involves a regression process to evaluate the approximate values of the partial topology parameters, i.e. the line susceptances and the conductances, while the second step involves obtaining their exact estimates.

1) Step-I: Parameter Evaluation through Regression

From (1)-(2), for a given number of nodes 'n', it is possible to write,

$$\begin{bmatrix} \frac{P_i}{|V_i|} & \frac{Q_i}{|V_i|} \end{bmatrix}^T = \begin{bmatrix} G_{i1}^{\#} & G_{i2}^{\#} & \cdots & G_{in}^{\#} \\ B_{i1}^{\#} & B_{i2}^{\#} & \cdots & B_{in}^{\#} \end{bmatrix} \begin{bmatrix} |V_1| \\ |V_2| \\ \vdots \\ |V_n| \end{bmatrix} \quad (3)$$

where,

$$G_{ij}^{\#} = \left(G_{ij} \cos\theta_{ij} + B_{ij} \sin\theta_{ij}\right)$$
$$B_{ij}^{\#} = -\left(G_{ij} \sin\theta_{ij} - B_{ij} \cos\theta_{ij}\right) \quad (4)$$

Initially, using the available smart meter measurements (i.e. real power, reactive power and the voltage magnitude) at different time stamps, the following matrices are formulated for 'K' instants of measurements,

$$[\mathbf{PV^K}] = \begin{bmatrix} \frac{P_1^{(1)}}{|V_1|^{(1)}} & \cdots & \frac{P_1^{(K)}}{|V_1|^{(K)}} \\ \vdots & \ddots & \vdots \\ \frac{P_r^{(1)}}{|V_r|^{(1)}} & \cdots & \frac{P_r^{(K)}}{|V_r|^{(K)}} \end{bmatrix}$$
$$[\mathbf{QV^K}] = \begin{bmatrix} \frac{Q_1^{(1)}}{|V_1|^{(1)}} & \cdots & \frac{Q_1^{(K)}}{|V_1|^{(K)}} \\ \vdots & \ddots & \vdots \\ \frac{Q_r^{(1)}}{|V_r|^{(1)}} & \cdots & \frac{Q_r^{(K)}}{|V_r|^{(K)}} \end{bmatrix} \quad (5)$$

The superscripts '*(1)*' to '*(K)*' represent the time instants of measurements, while the subscripts '*1*' to '*r*' represent the numbers corresponding to a node assuming that the smart meters are installed at 'r' nodes (r ∈ ℕ). Using (3),(5), the following expression can be written,

$$[\mathbf{PV^K}]_{r\times K} = \begin{bmatrix} G_{11}^{\#} & \cdots & G_{1n}^{\#} \\ \vdots & \ddots & \vdots \\ G_{r1}^{\#} & \cdots & G_{rn}^{\#} \end{bmatrix} \begin{bmatrix} |V_1|^{(1)} & \cdots & |V_1|^{(K)} \\ \vdots & \ddots & \vdots \\ |V_r|^{(1)} & \cdots & |V_r|^{(K)} \end{bmatrix} \quad (6)$$

A pseudo-inverse technique [23], is then used to compute the approximate values of '$G_{ij}^{\#}$' matrix as,

$$[\mathbf{G}^{\#}] = [\mathbf{PV^K}][\mathbf{V^K}]([\mathbf{V^K}][\mathbf{V^K}]^T)^{-1} \quad (7)$$

where, $[\mathbf{G}^{\#}]$ corresponds to the first matrix of the right-hand part of (6), while $[\mathbf{V^K}]$ is the corresponding second matrix. Likewise, '$B_{ij}^{\#}$' matrix is computed as,

$$[\mathbf{B}^{\#}] = -[\mathbf{QV^K}][\mathbf{V^K}]([\mathbf{V^K}][\mathbf{V^K}]^T)^{-1} \quad (8)$$

It may be noted that only the information of conductances and susceptances corresponding to the smart meter nodes is obtained from (7)-(8). The voltage angle 'θ_{ij}' in the distribution feeder, is usually within 0.1 rad, thereby, sin θ ≈ 0, cos θ ≈ 1. Therefore, the obtained values of '$G_{ij}^{\#}$' and '$B_{ij}^{\#}$' from (7)-(8), form the approximate values of 'G_{ij}' and 'B_{ij}', to be utilized in the succeeding step as depicted in Fig. 1.

2) Step-II: Parameter Evaluation through Newton-Raphson Analysis

In this step, the approximate values of conductances and the susceptances obtained in step-I, are used to obtain the corresponding exact values of the partial topology information (corresponding to the smart meter nodes) as depicted in Fig. 1. The Newton-Raphson (NR) method [17] is employed here, where the approximate conductances and susceptances serve as a fine initial start for this method. Using the available active and reactive power injection measurements, at the buses with smart meters, the change in the active and reactive power matrices are built as,

$$[\Delta\mathbf{P^K}] = \begin{bmatrix} P_1^{(1)} - P_{1c}^{(1)} & \cdots & P_1^{(K)} - P_{1c}^{(K)} \\ \vdots & \ddots & \vdots \\ P_n^{(1)} - P_{nc}^{(1)} & \cdots & P_n^{(K)} - P_{nc}^{(K)} \end{bmatrix}$$
$$[\Delta\mathbf{Q^K}] = \begin{bmatrix} Q_1^{(1)} - Q_{1c}^{(1)} & \cdots & Q_1^{(K)} - Q_{1c}^{(K)} \\ \vdots & \ddots & \vdots \\ Q_n^{(1)} - Q_{nc}^{(1)} & \cdots & Q_n^{(K)} - Q_{nc}^{(K)} \end{bmatrix} \quad (9)$$

where, the prefix 'c' denotes the calculated values. Initially, these real and reactive powers are calculated using the approximate susceptances and conductances. The Jacobian

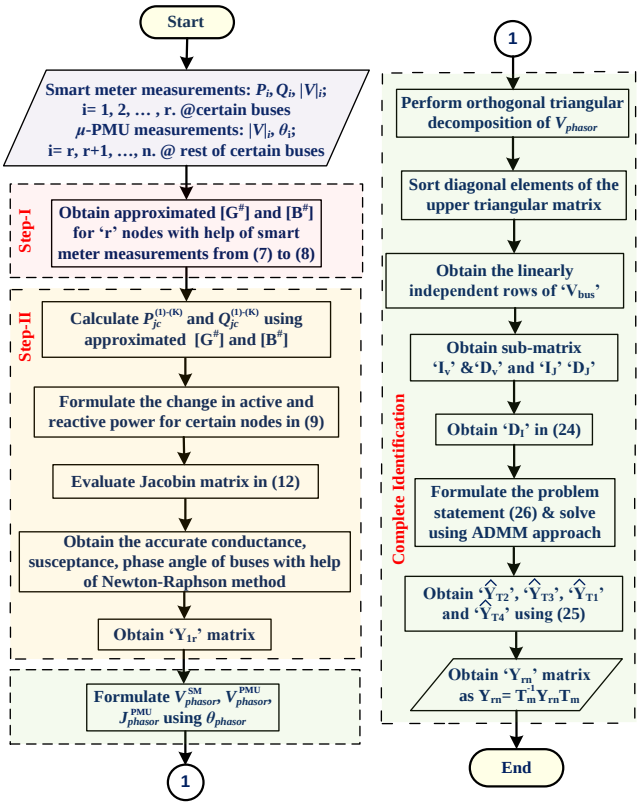

Fig. 1 Flow-chart of the presented framework for network identification

matrix [17] in the NR method is as,

$$\begin{bmatrix}\Delta\mathbf{P}\\ \Delta\mathbf{Q}\end{bmatrix}=\begin{bmatrix}\frac{\partial\mathbf{P}}{\partial\mathbf{g}} & \frac{\partial\mathbf{P}}{\partial\mathbf{b}} & \frac{\partial\mathbf{P}}{\partial\boldsymbol{\theta}}\\ \frac{\partial\mathbf{Q}}{\partial\mathbf{g}} & \frac{\partial\mathbf{Q}}{\partial\mathbf{b}} & \frac{\partial\mathbf{Q}}{\partial\boldsymbol{\theta}}\end{bmatrix}\begin{bmatrix}\Delta\mathbf{g}\\ \Delta\mathbf{b}\\ \Delta\boldsymbol{\theta}\end{bmatrix} \tag{10}$$

where,

$$\Delta\mathbf{g}=\begin{bmatrix}\boldsymbol{g_1}\\ \vdots\\ \boldsymbol{g_m}\end{bmatrix};\Delta\mathbf{b}=\begin{bmatrix}\boldsymbol{b_1}\\ \vdots\\ \boldsymbol{b_m}\end{bmatrix};\Delta\boldsymbol{\theta}=\begin{bmatrix}\theta_1^{(1)} & \dots & \theta_1^{(K)}\\ \vdots & \ddots & \vdots\\ \theta_n^{(1)} & \dots & \theta_n^{(K)}\end{bmatrix} \tag{11}$$

The problem (10), is solved using the pseudo-inverse [17] as,

$$\begin{bmatrix}\Delta\mathbf{g}\\ \Delta\mathbf{b}\\ \Delta\boldsymbol{\theta}\end{bmatrix}=\begin{bmatrix}\frac{\partial\mathbf{P}}{\partial\mathbf{g}} & \frac{\partial\mathbf{P}}{\partial\mathbf{b}} & \frac{\partial\mathbf{P}}{\partial\boldsymbol{\theta}}\\ \frac{\partial\mathbf{Q}}{\partial\mathbf{g}} & \frac{\partial\mathbf{Q}}{\partial\mathbf{b}} & \frac{\partial\mathbf{Q}}{\partial\boldsymbol{\theta}}\end{bmatrix}^{\dagger}\begin{bmatrix}\Delta\mathbf{P}\\ \Delta\mathbf{Q}\end{bmatrix} \tag{12}$$

The conductances, the susceptances as well as the voltage angles are updated as,

$$[\mathbf{g}\quad\mathbf{b}\quad\boldsymbol{\theta}]_u^T=[\mathbf{g}\quad\mathbf{b}\quad\boldsymbol{\theta}]^T+[\Delta\mathbf{g}\quad\Delta\mathbf{b}\quad\Delta\boldsymbol{\theta}]^T \tag{13}$$

The new values of the line parameters and the voltage angles are then used for the next NR iteration, while these iterations are carried out until the convergence point is reached. For the threshold for convergence, computation of the pseudo-inverse (†) as well as the Jacobian matrix, the reader is directed to [17]. A threshold is set for the topology modification, where the small values of conductances and susceptances are identified as wrong branches and thus eliminated. The NR iteration is run again whenever a branch is less than this threshold. the accuracy of the voltage angle estimation is also improved using a pseudo power flow conducted with the known information, before every iteration. The overall process to obtain the accurate network parameters is illustrated in Fig. 1.

C. Complete Topology Information with μ-PMU Measurements

The partial information of the line susceptances and conductances are obtained, using the smart meter measurements, by solving the NR method in section B-2. However, to obtain the complete information of the topology, the μ-PMU measurements are mandatory. As depicted earlier, for SM installed at buses '*1*' to '*r*', the information obtained from solving (12), are the elements of the true conductance and susceptance matrices, corresponding to the approximate matrices $[\mathbf{G}^{\#}]$ and $[\mathbf{B}^{\#}]$ in (6) and (7) respectively. Thus, as the 'G_{ij}' and 'B_{ij}' from the rows '*1*' to '*r*' are accurately known by step B-2, which implies that the top '*r*' rows of the bus admittance matrix are known accurately, *i.e.* from the system's bus admittance matrix (14), the submatrix '$\mathbf{Y_{1r}}$' corresponding to the matrix with first 'r' rows, is entirely known.

$$\mathbf{Y_{bus}}=\begin{bmatrix}Y_{1,1} & \cdots & Y_{1,n}\\ \vdots & \ddots & \vdots\\ Y_{r,1} & \cdots & Y_{r,n}\\ Y_{r+1,1} & \cdots & Y_{r+1,n}\\ \vdots & \ddots & \vdots\\ Y_{n1} & \cdots & Y_{nn}\end{bmatrix} \tag{14}$$

The matrix '$\mathbf{Y_{rn}}$' is the matrix with the last '*n-r*' rows of '$\mathbf{Y_{bus}}$' in (14), associated with the unknown values. Thus the main goal is to estimate the elements of the matrix '$\mathbf{Y_{rn}}$' using the available μ-PMU voltage phasor and the current phasor measurements. For a distribution network with '*n*' number of nodes, the admittance matrix is associated with the current injections at the '*n*' nodes and the voltages at the '*n*' nodes in the following way,

$$\begin{aligned}&[J_1(k)\quad J_2(k)\quad\dots\quad J_n(k)]^T\\ &=\mathbf{Y_{bus}}.[V_1(k)\quad V_1(k)\quad\dots\quad V_n(k)]^T\end{aligned} \tag{15}$$

It may be noted that the elements of the current injections vector are $J_{i|\mathrm{i=1,2,..,n}}$ and the nodal voltages vector are $V_{i|\mathrm{i=1,2,..,n}}$, both of which are the complex quantities *i.e.* phasors at a particular instant of time '*k*'. These phasors are obtained from the phasor measurement units installed in the network. The information available from the phasor measurement units are the time-stamped current and voltage phasors with nodes '*r*' to '*n*', which are given as,

$$\begin{aligned}\mathbf{V}_{\boldsymbol{phasor}}^{\boldsymbol{PMU}}&=\begin{bmatrix}V_{r+1}(1) & \cdots & V_{r+1}(K)\\ \vdots & \ddots & \vdots\\ V_n(1) & \cdots & V_n(K)\end{bmatrix}\\ \mathbf{J}_{\boldsymbol{phasor}}^{\boldsymbol{PMU}}&=\begin{bmatrix}J_{r+1}(1) & \cdots & J_{r+1}(K)\\ \vdots & \ddots & \vdots\\ J_n(1) & \cdots & J_n(K)\end{bmatrix}\end{aligned} \tag{16}$$

The indices in the brackets in (16) represent the voltage and current sample instants from '*1*' to '*K*'. With this available phasor information, the matrix '$\mathbf{Y_{rn}}$' needs to be estimated. For this purpose, the problem statement is formulated as,

$$\begin{aligned}\widehat{\mathbf{Y}}_{\mathbf{rn}}=argmin&\left\|\mathbf{Y_{rn}}.\underbrace{\begin{bmatrix}\mathbf{V}_{\boldsymbol{phasor}}^{\boldsymbol{SM}}\\ \mathbf{V}_{\boldsymbol{phasor}}^{\boldsymbol{PMU}}\end{bmatrix}}_{\mathbf{V_{phasor}}}-\mathbf{J}_{\boldsymbol{phasor}}^{\boldsymbol{PMU}}\right\|\\ &subject\ to\ \mathbf{Y_{rn}}\in\mathbf{S}^{(n-r)\times n}\end{aligned} \tag{17}$$

where,

$$\mathbf{V}_{\boldsymbol{phasor}}^{\boldsymbol{SM}}=\begin{bmatrix}V_1(1) & \cdots & V_1(K)\\ \vdots & \ddots & \vdots\\ V_r(1) & \cdots & V_r(K)\end{bmatrix} \tag{18}$$

The vector in (18) is the phasor vector of voltages corresponding to the buses with smart meters, *i.e.* buses '*1*' to '*r*'. The information of this vector is known from the measured magnitudes '$|V_i|$', while the angle information is also known, from (13). Therefore, the feasible solution to the problem statement (17) could be obtained from the available information. By solving (17), the accurate '$\mathbf{Y_{rn}}$' is obtained, while the accurate '$\mathbf{Y_{1r}}$' is acquired in section B-2, thereby, the complete information of '$\mathbf{Y_{bus}}$' matrix is obtained. This information depicts both the topology, along with the line parameters of the network. However, obtaining the '$\mathbf{Y_{rn}}$' matrix directly from (17) is challenging, owing to the sparsity in the matrix and the matrices '$\mathbf{V}_{\boldsymbol{phasor}}^{\boldsymbol{PMU}}$' and '$\mathbf{J}_{\boldsymbol{phasor}}^{\boldsymbol{PMU}}$' being rank-deficient matrices. Therefore, the procedure to obtain '$\mathbf{Y_{rn}}$' accurately is reported as follows.

Initially, the upper triangular elements of the admittance matrix are grouped in the function $G(\mathbf{Y_{rn}})$ as,

$$\begin{aligned}G(\mathbf{Y_{rn}})=[&Y_{r+1,1}\quad Y_{r+1,2}\quad\dots\quad Y_{r+1,n}\\ &Y_{r+2,2}\quad Y_{r+2,3}\quad\dots\quad Y_{r+2,n}\\ &Y_{r+3,3}\quad\dots\quad\dots\quad Y_{n,n}]\end{aligned} \tag{19}$$

A binary operator '$\boldsymbol{O}_X$' is formulated, that could convert the $G(\mathbf{Y_{rn}})$ to $vec(\mathbf{Y_{rn}})$, which implies that $vec(\mathbf{Y_{rn}})=\boldsymbol{O}_X\times G(\mathbf{Y_{rn}})$. Thus, (17) is rewritten using (19) as [10-11],

$$\begin{aligned}G(\widehat{\mathbf{Y}}_{\mathbf{rn}})=\underset{\mathbf{x}\in\mathbb{C}^{(n^2+n)/2\times1}}{argmin}&\left\|(\mathbf{V_{phasor}}\otimes\mathbf{1_n})\boldsymbol{O}_X.\mathbf{x}\right.\\ &\left.-vec(\mathbf{J}_{\boldsymbol{phasor}}^{\boldsymbol{PMU}})\right\|\end{aligned} \tag{20}$$

where, $\otimes$ represents Kronecker product.

Owing to the low-rank structure of the matrices (16), a transformation matrix '$\mathbf{T_M}$' (size: $n\times n$ matrix) is formulated, that separate the linearly independent rows from the linearly dependent rows as,

$$\mathbf{T_M}.\mathbf{V_{phasor}}=[\mathbf{I_V}\quad\mathbf{D_V}]^T \tag{21}$$

In (21) '$\mathbf{I_V}$' is a matrix with the '*p*' linearly independent rows of '$\mathbf{V_{phasor}}$' and '$\mathbf{D_V}$' with the remaining *'n-p'* rows of the '$\mathbf{V_{phasor}}$' matrix.

To obtain '$\mathbf{T_M}$', firstly, the orthogonal triangular decomposition of '$\mathbf{V_{phasor}}$' is done and the diagonal elements of the upper triangular matrix are sorted [10]. The overall process to obtain '$\mathbf{T_M}$' is illustrated in Fig. 1. Then, the first 'p' elements of the permutation matrix thus obtained, are selected as the indices of the linearly independent rows. The sub-matrices '$\mathbf{I_V}$' and '$\mathbf{D_V}$' are thus obtained and in the similar way, sub-matrices '$\mathbf{I_J}$' and '$\mathbf{D_J}$'corresponding to the '$\mathbf{J}_{phasor}^{PMU}$' are also obtained *i.e.*,

$$\mathbf{T_M}.\mathbf{J}_{phasor}^{PMU} = [\mathbf{I_J} \quad \mathbf{D_J}]^T \tag{22}$$

The transformation operation for the admittance matrix is evaluated from (21) and (22) as,

$$\mathbf{T_M}.\mathbf{J}_{phasor}^{PMU} = \underbrace{\left(\mathbf{T_M}.\mathbf{Y_{rn}}.\mathbf{T_M^{-1}}\right)}_{\begin{bmatrix}\mathbf{Y_{T1}} & \mathbf{Y_{T2}}\\ \mathbf{Y_{T3}} & \mathbf{Y_{T4}}\end{bmatrix}} \left(\mathbf{T_M}.\mathbf{V_{phasor}}\right) \tag{23}$$

As '$\mathbf{I_V}$' is a linearly independent vector, '$\mathbf{D_V}$' could be written as '$\mathbf{D_V} = D_I.\mathbf{I_V}$', where,

$$D_I \left(\triangleq \begin{bmatrix} D_{I1} & D_{I2} \\ D_{I3} & D_{I4}\end{bmatrix}\right) = \mathbf{I_V} \times pinv(\mathbf{D_V}) \tag{24}$$

where, $pinv$ represents Moore-Penrose pseudoinverse. Thus, from (21)-(24),

$$[\mathbf{I_J} \quad \mathbf{D_J}]^T = \begin{bmatrix}\mathbf{Y_{T1}} & \mathbf{Y_{T2}} \\ \mathbf{Y_{T3}} & \mathbf{Y_{T4}}\end{bmatrix}.[\mathbf{I_V} \quad \mathbf{D_V}]^T \tag{25}$$

Finally, the optimization problem (20) is reformulated and estimated admittance submatrices ($\hat{\mathbf{Y}}_{\mathbf{T1}}, \hat{\mathbf{Y}}_{\mathbf{T4}}$) is computed using (23)-(25) as [10-11],

$$\begin{aligned}&\left[G\left(\hat{\mathbf{Y}}_{\mathbf{T1}}\right) \quad G\left(\hat{\mathbf{Y}}_{\mathbf{T4}}\right)\right] \\ &= \underset{\mathbf{x}\in\mathbb{C}^{(n^2+n)/2\times 1}}{argmin} \Big\| [-(D_I \otimes D_I)\boldsymbol{O}_{D_{I1}} \quad \boldsymbol{O}_{D_{I4}}].\mathbf{x} \\ &- vec\left(\left(\mathbf{I_V} \times pinv(\mathbf{I_V})\right) - \left(pinv(\mathbf{I_V}) \times \mathbf{I_J}\right).D_I\right)\Big\|\end{aligned} \tag{26}$$

To simplify the problem statement (26), the elements of (26) are assigned to new variables as,

$$\mathbf{G}|_{L\times 1} = \left[G\left(\hat{\mathbf{Y}}_{\mathbf{T1}}\right) \quad G\left(\hat{\mathbf{Y}}_{\mathbf{T4}}\right)\right] \tag{27}$$

$$\boldsymbol{\Upsilon}|_{L\times L} = [-(D_I \otimes D_I)\boldsymbol{O}_{D_{I1}} \quad \boldsymbol{O}_{D_{I4}}] \tag{28}$$

$$\begin{aligned}\mathbf{V}|_{L\times 1} = vec\Big(&\left(\mathbf{I_V} \times pinv(\mathbf{I_V})\right) \\ &- \left(pinv(\mathbf{I_V}) \times \mathbf{I_J}\right).D_I\Big)\end{aligned} \tag{29}$$

The size 'L' in (27)-(29) can be identified as $(2(n-r)^2 - (2(n-r)+1).p + p^2)/2$. The rest of sub-matrices ($\hat{\mathbf{Y}}_{\mathbf{T2}}, \hat{\mathbf{Y}}_{\mathbf{T3}}$) can be obtained through (25). Therefore, from (26)-(29), the system at hand, is described through following equation,

$$\mathbf{V} = \boldsymbol{\Upsilon}.\mathbf{G} + \boldsymbol{\varepsilon} \tag{30}$$

where, '$\boldsymbol{\varepsilon}$' is a finite Gaussian measurement noise. For a single i^{th} row, (30) can be written as,

$$\mathbf{V_i} = \boldsymbol{\Upsilon_i}.\mathbf{G_i} + \boldsymbol{\varepsilon_i}|_{i=1,2,\ldots,L} \tag{31}$$

To obtain the '$\boldsymbol{\Upsilon_i}$' from the (31), the regression problem [24-25] is formulated using alternating direction method of multipliers (ADMM) approach as follow.

$$\begin{aligned}&\underset{\boldsymbol{\Upsilon_i}}{argmin}(1/2)\|\boldsymbol{\Upsilon_i}\mathbf{G_i} - \mathbf{V_i}\|_2^2 + \alpha\|\mathbf{z_i}\|_1 \\ &\text{subject to } \mathbf{G_i} - \mathbf{z_i} = 0\end{aligned} \tag{32}$$

where, α is a regularization parameter factor; $\mathbf{z_i}$ are typically weighted vector and intermediate vector, $\mathbf{z_i} \in \mathbf{R}^m$. Based on the formulation of the ADMM method [24-25], the Lagrange multiplier ($\boldsymbol{y_i}$) is incorporated into the existing formulated problem (32) as follows.

$$\begin{aligned}\boldsymbol{F}(\mathbf{G_i}, \boldsymbol{z_i}, \boldsymbol{y_i}) = &(1/2)\|\boldsymbol{\Upsilon_i}\mathbf{G_i} - \mathbf{V_i}\|_2^2 + \alpha\|\mathbf{z_i}\|_1 \\ &+ \boldsymbol{y_i^T}(\mathbf{G_i} - \mathbf{z_i}) + (\rho/2)\|\mathbf{G_i} - \mathbf{z_i}\|_2^2\end{aligned} \tag{33}$$

where, ρ is a positive penalty parameter. In ADMM method, $\mathbf{G_i}$ and $\mathbf{z_i}$ are updated in an alternating or sequential fashion, which accounts for the term alternating direction. The minimization problem is divided into two subproblems to reduce the computational burden and executes the minimization independently, unlike the Lasso framework [10, 17, 24-25]. The iterative steps of the ADMM algorithm are expressed as,

$$\mathbf{G}^{k+1} = \underset{\mathbf{G}}{argmin}\ \boldsymbol{F}(\mathbf{G_i}, \boldsymbol{z_i}, \boldsymbol{y_i}) \tag{34}$$

$$\boldsymbol{z}^{k+1} = \underset{\boldsymbol{z}}{argmin}\ \boldsymbol{F}(\mathbf{G_i}, \boldsymbol{z_i}, \boldsymbol{y_i}) \tag{35}$$

$$\boldsymbol{y_i^{k+1}} = \boldsymbol{y_i^k} + \mathbf{G_i^{k+1}} - \boldsymbol{z_i^{k+1}} \tag{36}$$

The iteration (34)-(36) is updated until the stopping criterion is satisfied. The stopping criterion is defined as,

$$\begin{aligned}\left\|\mathbf{G_i^k} - \boldsymbol{z_i^k}\right\|_2 &\le \mu_{abs} + \mu_{rel} max\left(\left\|\mathbf{G_i^k}\right\|_2, \left\|\boldsymbol{z_i^k}\right\|_2\right) \\ \rho\left\|\boldsymbol{z_i^k} - \boldsymbol{z_i^{k+1}}\right\|_2 &\le \mu_{abs} + \mu_{rel}\rho\left\|\boldsymbol{y_i^k}\right\|_2\end{aligned} \tag{37}$$

where, μ_{abs} and μ_{rel} are absolute tolerance, relative tolerance, respectively.

III. Results and Discussions

To validate the effectiveness of the presented ADMM based network identification framework, the benchmarked IEEE 13-bus and IEEE 123-bus feeders are considered herein with a coupled household load. The Electric Power Research Institute (EPRI®) has developed the open distribution system simulator (OpenDSS®) software, which facilitates the input/output information to study the dynamics of the benchmarked distribution feeder. The main advantage of OpenDSS® platform is that it is capable to perform multi-phase power flow, unbalanced power flow analysis, fault/event analysis, and stability analysis, unlike MATPower® and PowerWorld® simulator platform. Fig. 2 shows the detailed process of an iterative procedure of MATLAB® software with OpenDSS® platform. The component object model (COM) interface platform is used to communicate between OpenDSS and MATLAB® software. The detailed script of location and rating of integrated renewable energy sources, variation in branch parameters, type of events, etc., are written and recorded in the MATLAB® environment and this script is processed as input to the OpenDSS® platform. Likewise, the event-logger of the OpenDSS® platform also has an inherent feature to track/record the operation, control action, switching operation, and event for the given network. The voltage measurement is directly obtained from the node. The current measurement is obtained by taking the difference between the net injected current and net outgoing current at a certain bus. A command-separated value (.csv) report of the voltage-current dataset is obtained and processed into the MALTAB® software to accomplish the identification objectives. The salient points of the iterative procedure are depicted in Fig. 2.

The detailed configuration of the modified IEEE 13-bus system is illustrated in Fig. 3. From Fig. 3, it is easy to observe that the IEEE 13-bus system is highly unbalanced lateral as each phase is not connected with all buses. For the reliability of the electric power supply, the normally open (NO) and normally closed (NC) breakers are coupled between 692-680 and 692-671 buses as depicted in Fig. 3. The detailed installation of the smart meter and μ-PMUs are demonstrated in Fig. 3. Based on optimal location, the SMs (e.g., 611, 645, 646, 652, 671, 680, 684) and μ-PMUs (e.g., 632, 633, 634, 650, 675) are considered herein to suffice the identification objectives. The necessary data at each bus of the IEEE 13-bus system is acquired from the OpenDSS® software, then, processed further in the MATLAB® platform. The real-time measurements of the local load profile for the benchmarked IEEE 13-bus system are acquired from the

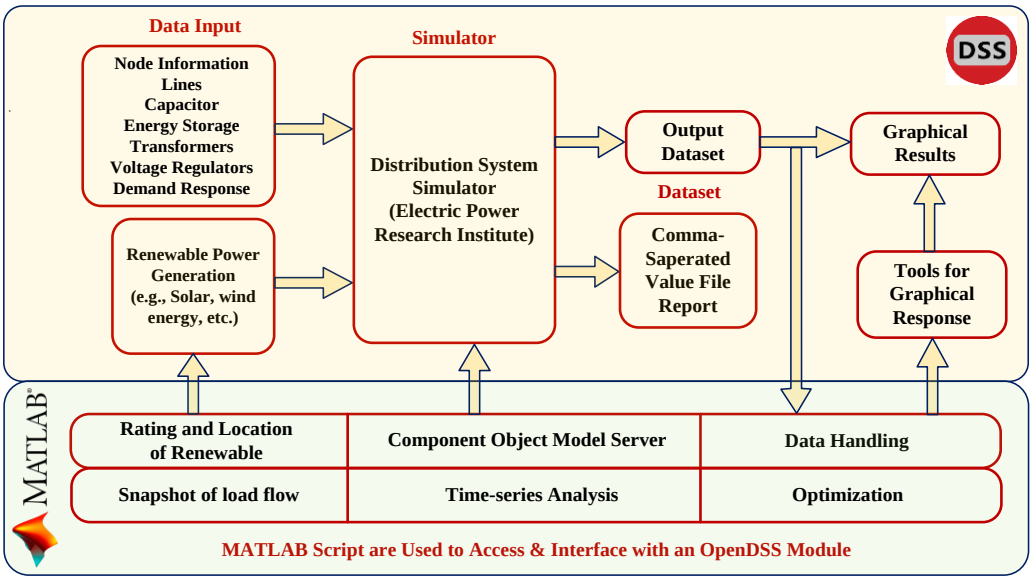

Fig. 2 Iterative framework between OpenDSS® and MATLAB® to accomplished network identification objectives

Autonomous Decentralised Renewable Energy Systems (ADRES) project repository [26-27]. The performance of the network identification algorithm is tested under several operating scenarios such as basic identification, identification with the consideration of noise in the measurements, impact of change in standard deviation in measurements, and identification under a change in the system configuration. The detailed analysis of the presented framework with various cases is analyzed as follows.

Case-I Basic Identification of Topology

Figs. 4 (a-c) demonstrate the basic identification of the modified IEEE 13-bus system. As smart meter data and μ-PMUs data are obtained from the defined buses, the presented ADMM algorithm segregates the data based on the type of measurements and identifies the network configuration using (7)-(8), (13) and (31). Fig. 4 (a) shows the identification of phase-'a' of the given IEEE 13-bus low-voltage distribution system. From Fig. 4 (a), it can be observed that the identification error in the admittance matrix is quite low in the range of 10^{-1}. Similarly, the identification in the admittance matrix for the phase-'b' and phase-'c' are illustrated in Figs. 4 (b-c). The typical value of error in identification is very low as the presented method provides robust identification and has good accuracy due to having insusceptibility against poor conditioning. The detailed analysis of the identification error in conductance and susceptance of each branch (e.g. for phase-'a', phase-'b', and phase-'c') is plotted in Figs. 4 (d-f). It can be easily seen that the error in estimated parameters is achieved within 2%.

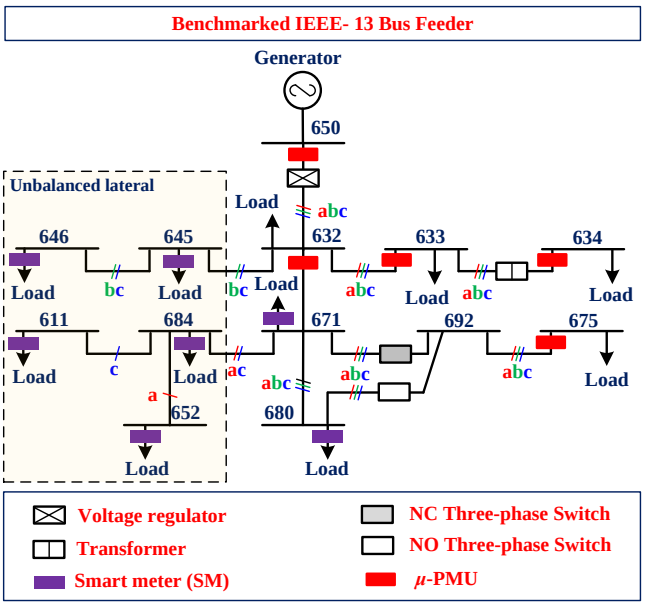

Fig. 3 Detailed schematics of the benchmarked IEEE 13-bus system

Case-II Performance of Network Identification with Consideration of Noise in SM Measurements

Fig. 5 (a) and Fig. 5 (b) demonstrate the robust

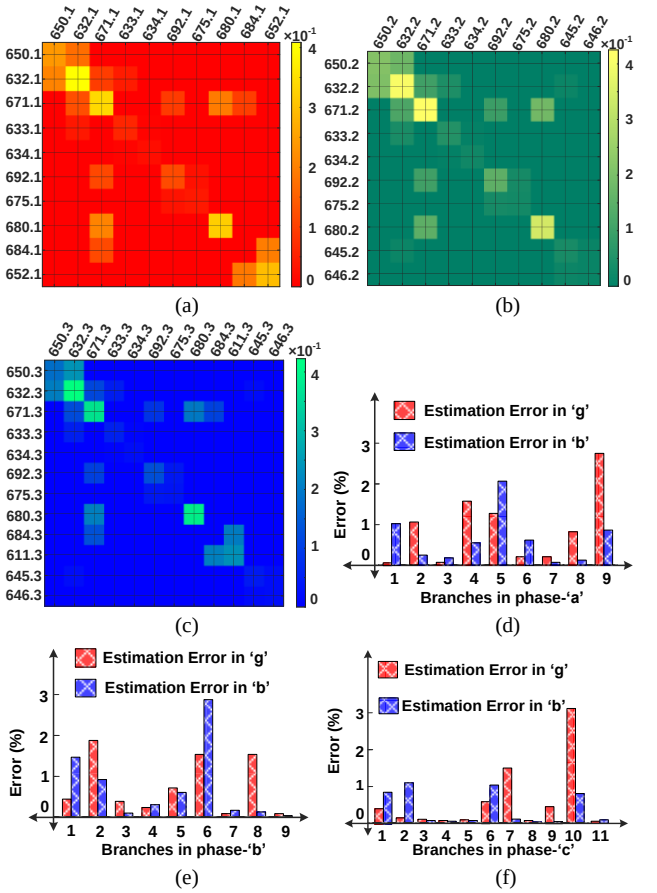

Fig. 4 Estimation of branch parameters of for the IEEE 13-bus feeder using presented framework (a-c) Coloured representation of individual phase admittance matrix estimation errors (a) Phase-'a', (b) Phase-'b' and, (c) Phase-'c', (d-f) Relative error of the estimated conductance and susceptance of each of the branches of (d) Phase-'a', (e) Phase-'b', (f) Phase-'c'

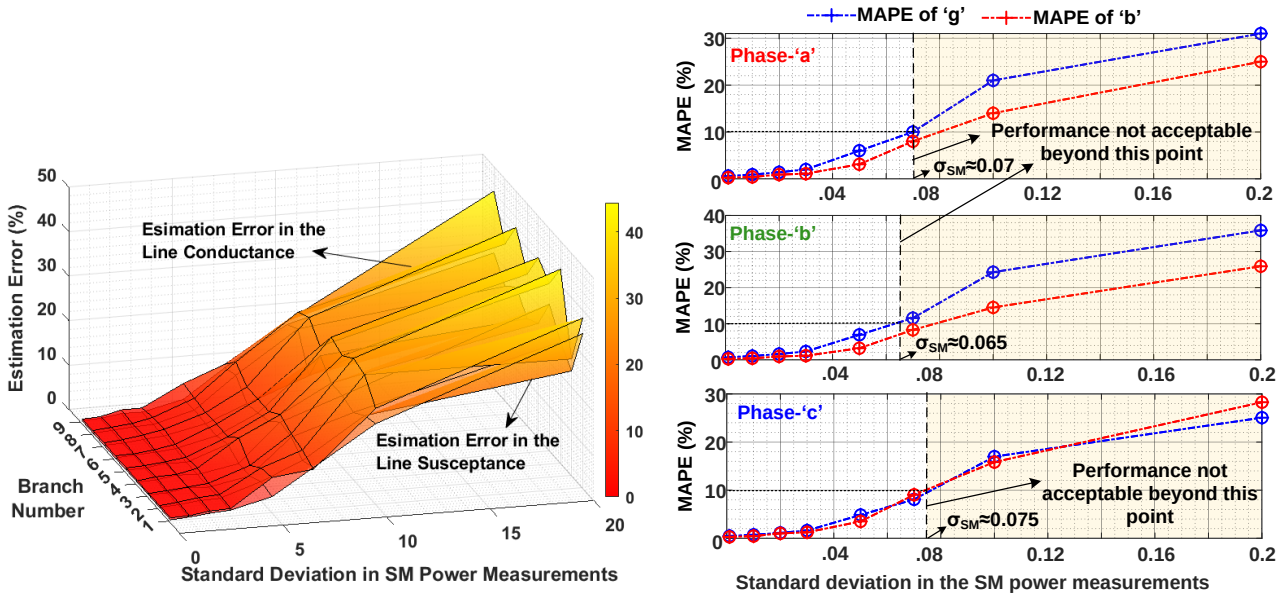

(a) (b)

Fig. 5 Estimation error of the algorithm for different noise levels in the SM power measurements (a) 'g' and 'b' error variation with the standard deviation in each of phase-'a' branches, (b) MAPE variation of 'g' and 'b' in all three phases

performance of the network identification algorithm with consideration of noise in the SM measurements. Fig. 5 (a) shows the illustrative 3-D heat map of estimation error (%) of each branch versus standard deviation in SM measurements. It is easy to observe that identification error is quite noticeably low for having a low standard deviation of SM measurements. The Newton-Raphson algorithm (9)-(13) has inherent advantages of swiftness and quadratic convergence rate. As standard deviation is increased in the SM measurements, the identification error is considerably increased as depicted in Fig. 5 (a). Furthermore, the mean absolute percentage error for the estimated branch parameters of each phase is analyzed in Fig. 5 (b) with the variation of standard deviation in the SM measurements. The 'blue' and 'red' color graph indicates the 'mean absolute percentage error' for estimated conductance and susceptance, respectively. The presented ADMM based network identification algorithm provides accurate results as it follows the decomposition-coordination procedure and local-subproblems (34)-(36) are coordinated to find a solution to a large global problem. In general, the typical variation in the range of 10% is observed in the estimated branch parameters when any dynamic reconfiguration/event has occurred in the system. Therefore, it may lead to an indication of the change in the network configuration for having erroneous results in estimated conductance and susceptance parameters. Hence, the limit line is chosen at 10% in the maximum absolute percentage error (MAPE) graph in Fig. 5 (b). One can be easily observed that the permissible standard deviation is found in range of 0.07 for the satisfactory identification as estimation error breaches the maximum allowable change (10%) in branch parameters afterwards.

Case-III Performance of Network Identification with Consideration of Noise in μ-PMU Measurements

Fig. 6 and Fig. 7 demonstrates the robustness of the presented algorithm to suffice the identification objectives with the consideration of noise in the μ-PMU measurements. Fig. 6 (a) shows the illustrative 3-D heat map of estimation error (%) of each branch versus standard deviation in μ-PMU measurements. It shows that the identification error is quite low for having a small value of the standard deviation. The presented algorithm has better noise rejection capability [24-25], thereby, the identification objective is not compromised as depicted in Fig. 6 (a) As the standard deviation is increased in the measurements, the identification error is increased as depicted in Fig. 6 (a). The detailed error analysis using 'mean absolute percentage error' is analyzed in Fig. 6 (b) for the estimated conductance and susceptance of each branch. It can be easily observed that the permissible standard deviation is accomplished within the range of 3×10^{-3} for the satisfactory operation of the identification algorithm as estimation error breaches the maximum allowable change (10%) in branch parameters afterward. The salient point of the network identification is described in Fig. 6 (b). Fig. 7 shows the required number of iterations to estimate the accurate branch parameters with a variation in the standard deviation. The presented algorithm has a better convergence rate with a low number of iterations, which is explained as follows. The Newton-Raphson algorithm has a quadratic converge rate and obtained information is processed further to estimate the branch parameters through the ADMM algorithm. In the ADMM algorithm, it explicitly targets the minimization problem by splitting it into two distinct objectives and provides better optimization [24-25]. In addition, the presented ADMM algorithm naturally decouples the non-smooth term from the smooth term, which is computationally advantageous over state-of-art algorithms [24-25, 28-30]. Furthermore, the actual effects on the identification of the admittance matrix are illustrated in Fig. 8. One can easily notice that there is a significant error in the identified branch parameters in the range of ten. Therefore, this estimation error in the admittance matrix will propagate in the state estimation and will lead to the non-optimal operation of the system.

Case-IV Effect of Change in Standard Deviation with Number of μ-PMUs

The estimation of branch parameters with wide variations of standard deviation for different numbers of μ-PMUs are analyzed in Figs. 9 (a-b). Fig. 9 (a) shows the identification error for having three μ-PMUs in the IEEE 13-bus (e.g., 632,

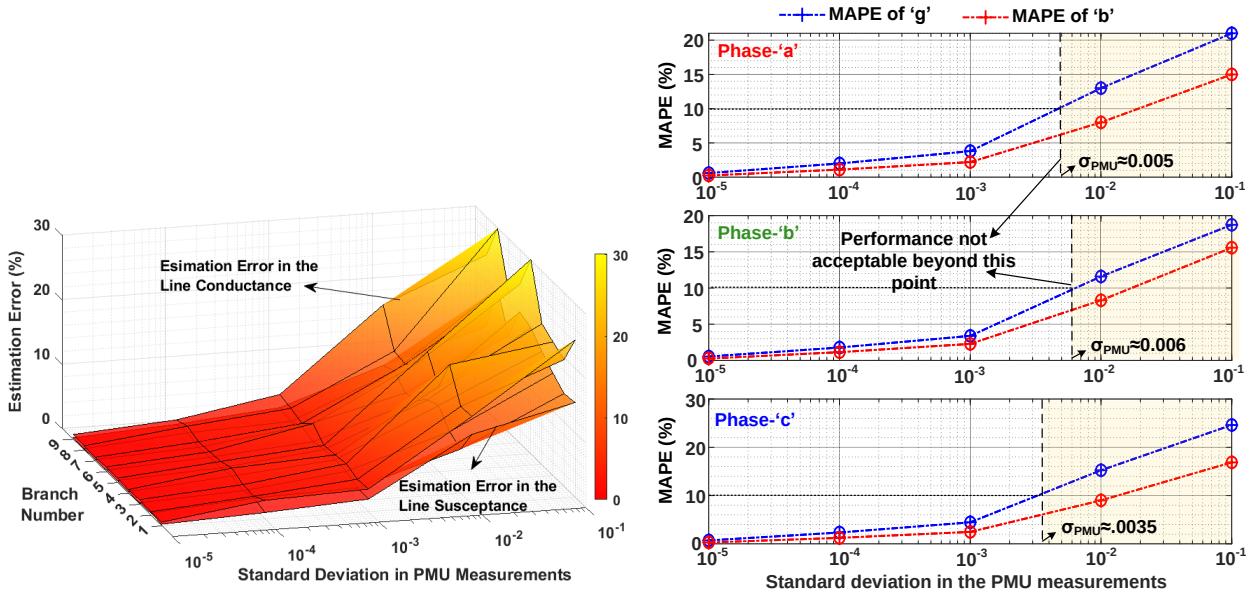

(a) (b)

Fig. 6 Estimation error of the algorithm for different noise levels in the μ-PMU measurements (a) 'g' and 'b' error variation with the standard deviation in each of phase-'a' branches, (b) MAPE variation of 'g' and 'b' in all three phases

650, 675) low-voltage distribution system. The identification error for having three μ-PMUs is accomplished within range of 40 with consideration of standard deviation of 10^{-1} in the measurements. The identification error can be reduced by having more numbers of μ-PMUs in the system as depicted in Fig. 9 (b). The identification performance is shown in Fig. 9 (b) for having four μ-PMUs in the system (e.g., 632, 634, 650, 675). The identification error is achieved within the range of 30 with consideration of a standard deviation of 10^{-1} in the measurements. The mean absolute percentage error for parameter identification is analyzed for having three, four, and five μ-PMUs in the IEEE 13-bus feeder. As the number of μ-PMUs increases, the identification error is reduced, however, it is a trade-off between accuracy and overall cost of the network monitoring system.

Case-V Performance of Network Identification with Change in Network Configuration

Figs. 10 (a-c) show the identification of events in the IEEE 13-bus distribution system with an altered status of the three-phase breaker between the buses 671-692 and 680-692. These results are captured by taking the difference of estimated admittance matrix, which are computed before the event and after the event, in the network. Figs. 10 (a-c) show the amount of change in the admittance matrix with the specific bus number for each phase, respectively. It is worth noticing that

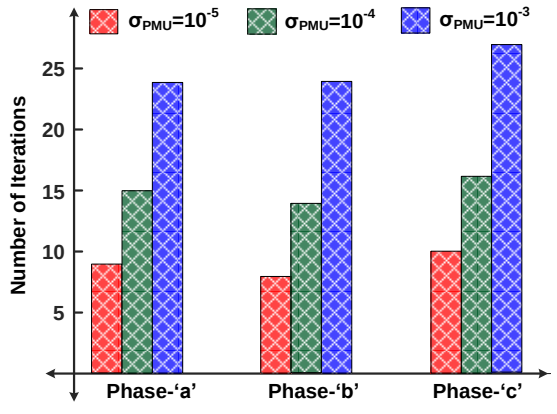

Fig. 7 Number of iterations for convergence of the algorithm for three different μ-PMU standard deviations

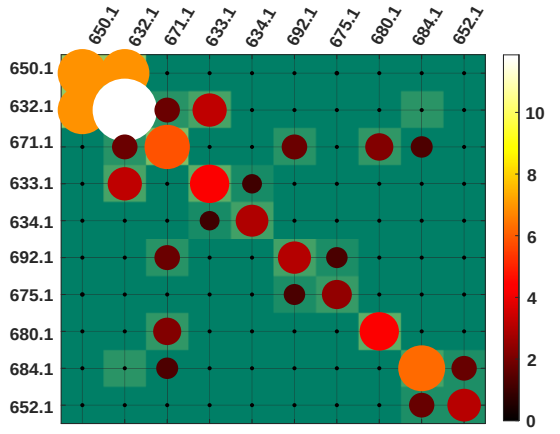

Fig. 8 Effect of change in standard deviation in μ-PMU measurements on the phase-'a' admittance matrix error

the change is symmetrical (e.g., $Y_{671\text{-}692}$, $Y_{671\text{-}671}$, and $Y_{692\text{-}671}$) in the heat map as the three-phase breaker between the buses 671-692 is altered from its nominal status. Likewise, the change in the conductance and susceptance (e.g., $Y_{680\text{-}692}$, $Y_{680\text{-}680}$, and $Y_{692\text{-}680}$) of the corresponding buses are also detected in Figs. 10 (a-c) as the three-phase breaker between the buses 680-692 is altered from its nominal status. The typical change in the estimated admittance matrix is about to be in the range of 15 to 20 for each phase. The detailed change in the conductance and susceptance of the estimated admittance matrix is analyzed in Figs. 10 (d-f). In addition, the typical changes in conductance and susceptance values are captured through its variation in the estimated conductance and susceptance at two different instants (e.g., before and after the event). For ease of understanding, the change in branches 671-692 has been analyzed in Figs. 10 (d-f) as the branches 680-692 did not exist before the event. Hence, the typical variation of the branch parameters (e.g., 671-692) for each phase is illustrated in Figs. 10 (d-f).

Case-VI Performance of Network Identification with Only μ-PMUs Measurement

Figs.11 (a-c) show the performance of the system with only the presence of μ-PMU measurements (i.e., placed at all buses) for the given benchmarked IEEE 13-bus feeder. The

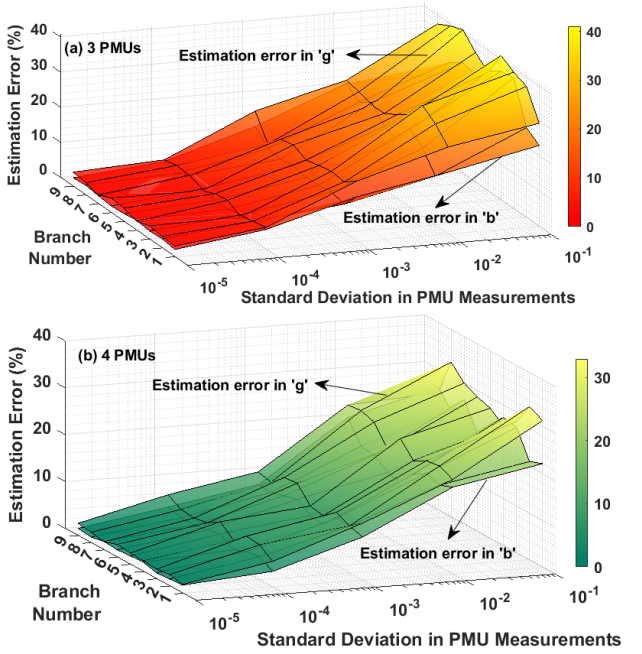

Fig. 9 Variation of the estimation error of 'g' and 'b' in various phase-'a' branches with optimal μ-PMU locations (a) With 3 μ-PMUs and, (b) With 4 μ-PMUs

error in the estimated nodal admittance matrix is plotted in Figs. 11 (a-c). It can be easy to observe that identification error for phase- 'a' is quite low and attained within satisfactory limits as depicted in Fig. 11 (a). As these measurements include the voltage phase angle and current phase angle, the identification computational time quite low (i.e., phase angle of the distribution buses is not required to estimate through the Newton-Raphson method). Likewise, the network identification for phase-'b' and phase-'c' is illustrated in Figs. 11 (b-c). Hence, the presented ADMM algorithm-based framework effectively identifies the network structure. Therefore, the identification task can be accomplished quickly as compared to nominal topology identification.

Case-VIII Performance of Network Identification for Benchmarked IEEE 123-Bus Feeder

Fig. 12 (a) shows the schematics of the benchmarked IEEE 123-bus feeder. The detailed configuration, connection, and location of power system components (e.g., voltage regulator, switch, transformer, etc.) are described in Fig. 12 (a). The real-time measurements of the local load profile (e.g., the household electrical load, commercial load, and industrial load) for the benchmarked IEEE 123-bus system are acquired from the Autonomous Decentralised Renewable Energy Systems (ADRES) project repository [26-27]. For simplicity, the identified network for phase-a of the IEEE 123-feeder is demonstrated in Fig. 12 (b). It shows the error in the estimated nodal admittance matrix of the identified system configuration. One can easily notice that identification error in the admittance matrix (e.g., conductance and susceptance) is quite low and accomplished within permissible limits as depicted in Fig. 12 (b). The presented framework provides swift network identification as compared to the state-of-art least absolute shrinkage and selection operator (Lasso) algorithm. The advantage of the presented framework lies in the formulation of optimization problem [28-30] and an update of search variable can be decomposed, which means

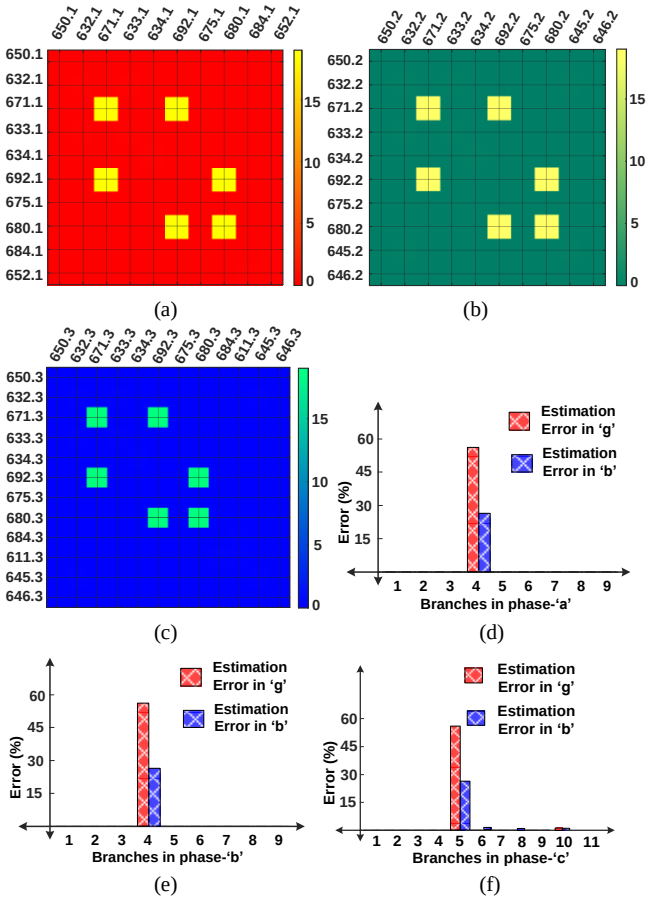

Fig. 10 Coloured representation of individual phase admittance matrix estimation errors, following the switching event (a) Phase-'a', (b) Phase-'b' and, (c) Phase-'c', (d-f) Relative error of the estimated conductances and susceptances of each of the branches in three phases, following the switching event for phase-'a', phase-'b' and phase-'c'

the problem can be easily parallelized or scalable even for large network/topology. Hence, the presented framework works satisfactorily for the benchmarked IEEE 123-bus feeder, and it successfully illustrates the scalability and efficacy for the large feeder system.

Case-VII Performance of Network Identification with Integration of Renewable Energy Sources

Fig. 13 shows the performance of the system with the presence of renewable energy sources. The location of the renewable energy sources at certain buses is given as follows: 650, 632, 671, 633, 680, 684, and 652. Certain points are needed to be clear to understand the impact of renewable energy sources on the network identification objectives. The heat bar in the left-hand side of the heat map manifests the error in the estimated nodal admittance matrix before the connection of the renewable energy sources. Likewise, the bubble size and bubble colour represent an increment of identification error in the estimated nodal admittance matrix with the presence of renewable energy sources. One can observe that the identified error in an estimated admittance matrix is accomplished within the range of 0.35, which is quite lower than the nominal operating scenario. It is easy to notice that most of the bubble in the heat map is orange, yellow, and sky-blue colour, which denotes a minor increment in identification error with integration of renewable energy sources Nonetheless, the presented framework identifies the network configuration satisfactorily with the presence of the renewable energy sources.

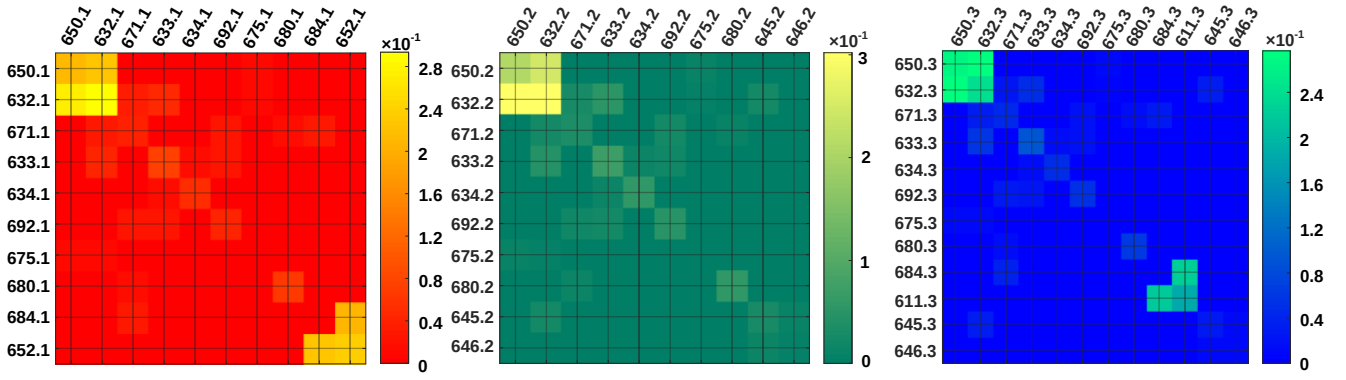

(a) (b) (c)

Fig. 11 Performance of the system with the presence of μ-PMU device (a) Phase-'a', (b) Phase-'b' and, (c) Phase-'c'

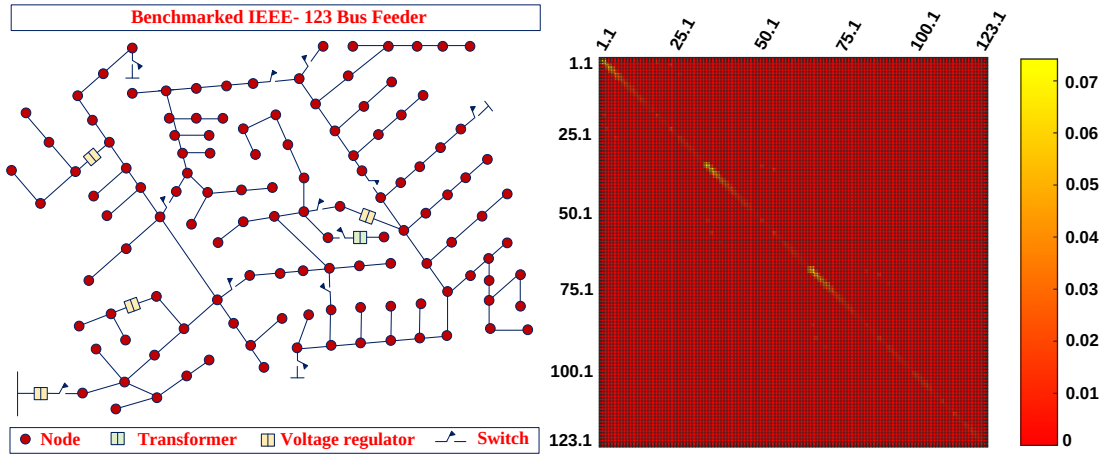

(a) (b)

Fig. 12 Network identification of the IEEE 123-bus feeder using presented framework (a) Detailed schematics of the benchmarked IEEE 123-bus system, (b) Coloured representation of phase admittance matrix estimation errors for phase-'a'

IV. Comparative Performances

The comparative performance is carried out between the presented algorithm and state-of-art algorithms [10-11, 17]. The two distinct scenarios are considered to evaluate the effectiveness of the presented framework over the state-of-art framework. Firstly, the comparative performance is carried out on the benchmarked IEEE 33-bus balanced feeder with the presence of Gaussian noise. The location of smart meters and μ-PMUs are given as follows: μ-PMUs are connected at certain buses of the IEEE-33 bus feeder [31] such as 16, 17, 18, 22, 30, 31, 32, and 33; whereas smart meter is connected at rest of the buses. Secondly, the event detection is carried out on the benchmarked IEEE 13-bus unbalanced feeder. The detailed analysis is described as follows.

Case-I Comparative Performance Between Presented Framework and State-of-art Framework for Balanced Feeder

Figs. 14 (a-b) and Figs. 15 (a-b) show the response of the state-of-art framework [17] to identify the benchmarked IEEE 33-bus feeder structure with the presence of Gaussian noise in the measurements. Fig. 14 (a) shows that identification error is attained within the range of 0.7 using the state-of-art framework [17], which is quite higher than basic network identification. Nevertheless, the performance of the identification is attained within permissible limits and the tracking of branch parameters is illustrated in Fig. 15 (a). It shows that the identification of the branch parameters (e.g., conductance and susceptance) fall within the range of 1 % to 4 %. The performance of the presented framework to identify the topology structure is described in Fig. 14 (b) and Fig. 15 (b). It is easy to notice that the error in the estimated nodal

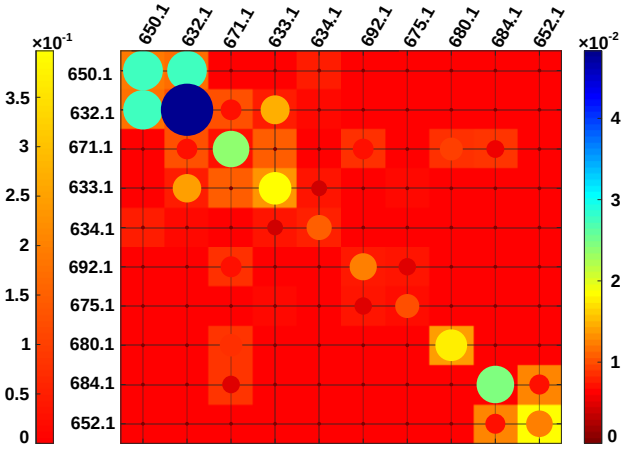

Fig. 13 Network identification of the IEEE 13-bus feeder with the presence of renewable energy sources

admittance matrix is quite low (e.g., 0.25) as compared to the state-of-art framework [17], which is clearly described in Fig. 14 (a) and Fig. 14 (b). The tracking performance of the branch conductance and susceptance is demonstrated in Fig. 15 (b). In contrast with state-of-art framework [17], it shows that presented framework has better estimation accuracy as the estimation error is accomplished within the range of 0.5 % to 2 %. Hence, the presented framework provides an excellent response as compared to the state-of-art framework [17].

Case-II Comparative Performance Between Presented Framework and State-of-art Framework for Unbalanced Feeder

Figs. 16 (a-b) shows the performance of the network identification with the steady-state estimation of branch

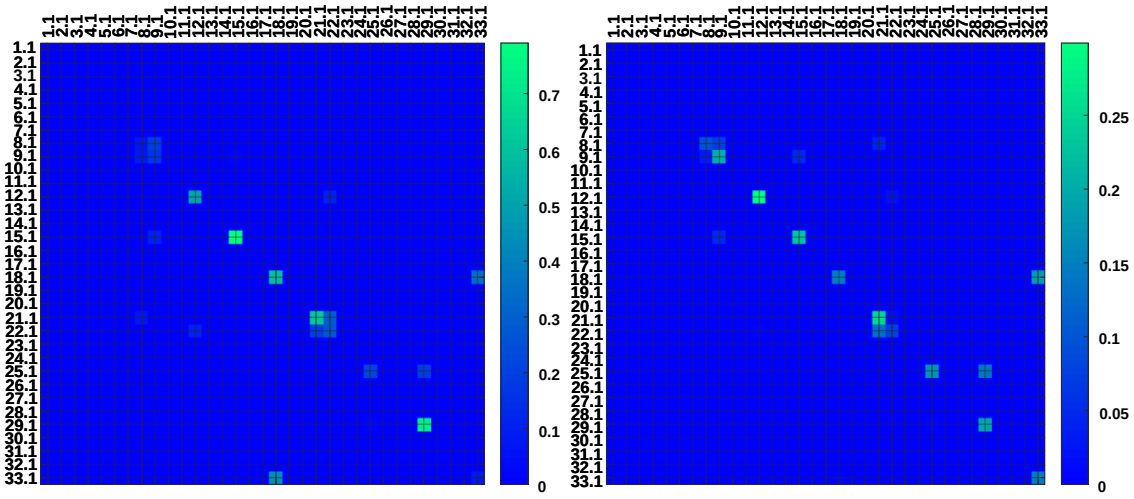

(a) (b)

Fig. 14 Comparative performance of the network identification of the benchmarked IEEE 33-bus feeder with the presence of Gaussian noise (a) Heat map of identification error using state-of-art framework [17], (b) Heat map of identification error using presented framework

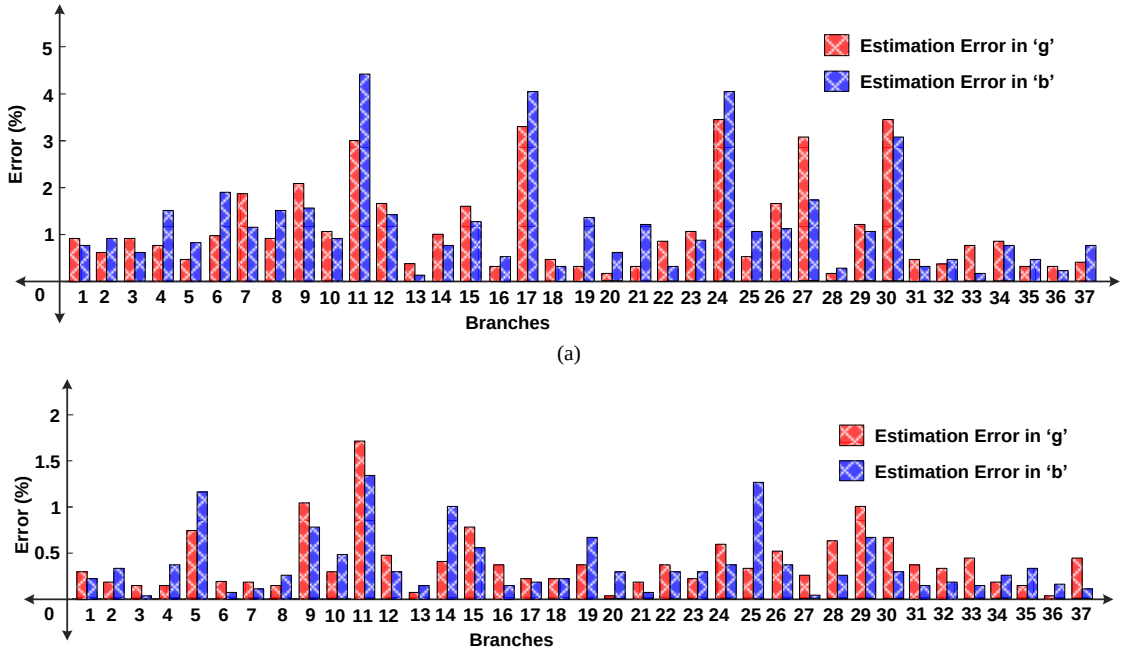

(a)

(b)

Fig. 15 Comparative performance of the network identification of the benchmarked IEEE 33-bus feeder with the presence of Gaussian noise (a) Tracking performance of conductance and susceptance of branch parameters using state-of-art framework [17], (b) Tracking performance of conductance and susceptance of branch parameters using presented framework

parameters variation of the branch parameters (e.g., 10% variation in branch 671-692). Fig. 16 (a) shows the network identification using the state-of-art algorithm [11] for the revised branch parameters. It shows that identification error using a state-of-art algorithm [11] in the estimated branch parameter of phase-'a' is found in the range of 3% to 6% as depicted in Fig. 16 (a). In contrast with the state-of-art [11] method, the presented algorithm estimates the updated branch parameters of phase-'a' with the estimation error in the range of 1% to 2% as illustrated in Fig. 16 (b). Furthermore, the comparative analysis between several methods [10-11, 17, 22] is described in Table-II. It shows that the algorithm [22] is not robust with respect to noise, unable to identify the change in branch parameters, and not feasible to identify the unbalanced network. Likewise, the graphical and comprehensive model [4, 6] fails to identify the network parameters and system configuration under unbalanced or noisy measurements. However, Lasso and Newton-Raphson algorithms [11, 17] are robust to the input noise and capable to identify the change in branch parameters with help of μ-

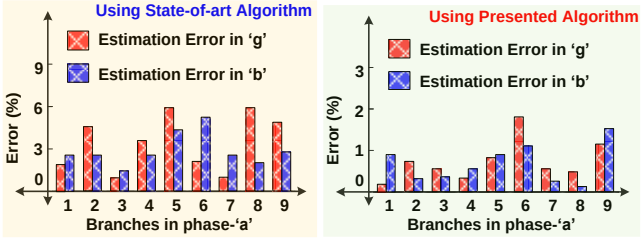

(a) (b)

Fig. 16 Comparative performances between state-of-art algorithm [10-11] and presented algorithm under variation of branch parameters

PMUs and smart meter measurements, respectively. However, they both fail to accomplish the network identification objectives when both measurements are available from the network. In contrary to the state-of-art methods [4, 6, 10-11, 17, 22], the presented algorithm copes up with both non-synchronous and synchronous measurements, robust with respect to noise, capable to identify the branch parameters even under an unbalanced network, etc. The salient points of various algorithms are described in Table-II.

TABLE-II COMPARISONS OF THE PRESENTED FRAMEWORK WITH EXISTING FRAMEWORKS

Description	[22]	[10-11]	[17]	Presented Algorithm
Type of algorithm	MIQP	Lasso	NR	ADMM
Identification with hybrid dataset	Not feasible	Not feasible	Not feasible	Feasible
Robustness	No	Yes	Yes	Yes
Accuracy	Average	Good	Relatively good	Better
Identification in unbalanced network	Not feasible	Feasible	Not feasible	Feasible
Identification with variation in branch parameters	Not feasible	Feasible	Feasible	Feasible

V. CONCLUSIONS

In this article, the alternating direction method of multipliers-based framework is presented herein to acquire the detailed network information with help of μ-PMU and SM measurements. The presented framework suffices the manifold identification objectives such as accurate estimation of the network structure, branch parameters, change in branch parameters, and change in the network configuration for low-voltage distribution feeder. In contrast with the state-of-art algorithms, the ADMM based framework has several advantages such as good accuracy, better convergence rate, etc. Simulation results confirm the effectiveness of the presented algorithm on the highly unbalanced IEEE 13-bus feeder with distinct operating scenarios. Accordingly, the case study shows that the presented algorithm has provided robust identification of the network configuration and branch parameters and accomplished the estimation error within satisfactory limits even with the consideration of the standard deviation in μ-PMU and SM measurements. The scalability and efficacy of the presented framework have been validated through the benchmarked large-scale IEEE 123-bus feeder. In addition, the presented framework has effectively accomplished the network identification objectives even with the presence of renewable energy sources. In order to validate the efficacy of the presented algorithm, the comparative performance has been carried out on the benchmarked IEEE 13-bus and IEEE 33-bus feeders, and it has outperformed network identification even under variation of the branch parameter and with the presence of Gaussian noise, unlike the state-of-art algorithms. In essence, the presented work will be very helpful to the network operator to accomplish the optimal operation of the distribution feeder.

REFERENCES

[1] W. Yao, S. You, W. Wang, *et al*., "A fast load control system based on mobile distribution-level phasor measurement unit," *IEEE Trans. Smart Grid*, vol. 11, no. 1, pp. 895-904, Jan. 2020.

[2] A. Prostejovsky, O. Gehrke, A. Kosek, *et al*., "Distribution line parameter estimation under consideration of measurement tolerances," *IEEE Trans. Ind. Informat.*, vol. 12, no. 2, pp. 726-735, April 2016.

[3] Y. Wang, Q. Chen, T. Hong, *et al*., "Review of smart meter data analytics: applications, methodologies, and challenges," *IEEE Trans. Smart Grid*, vol. 10, no. 3, pp. 3125-3148, May 2019.

[4] M. Babakmehr, M. Simões, M. Wakin, *et al*., "Compressive sensing-based topology identification for smart grids," *IEEE Trans. Ind. Informat.*, vol. 12, no. 2, pp. 532-543, April 2016.

[5] J. Xu, Z. Wu, X. Yu, *et al*., "Robust faulted line identification in power distribution networks via hybrid state estimator," *IEEE Trans. Ind. Informat.*, vol. 15, no. 9, pp. 5365-5377, Sept. 2019.

[6] D. Deka, M. Chertkov and S. Backhaus, "Joint estimation of topology and injection statistics in distribution grids with missing nodes," *IEEE Trans. Control Netw. Syst.*, vol. 7, no. 3, pp. 1391-1403, Sept. 2020.

[7] S. Lotfifard, "Sparse sensing platform for line-outage identification in multiarea power systems," *IEEE Trans. Ind. Informat.*, vol. 13, no. 3, pp. 947-955, June 2017.

[8] Z. S. Hosseini, A. Khodaei and A. Paaso, "Machine learning-enabled distribution network phase identification," *IEEE Trans. Power Syst.*, vol. 36, no. 2, pp. 842-850, March 2021.

[9] J. Yu, Y. Weng and R. Rajagopal, "PaToPa: A data-driven parameter and topology joint estimation framework in distribution grids," *IEEE Trans. Power Syst.*, vol. 33, no. 4, pp. 4335-4347, July 2018.

[10] O. Ardakanian, Y. Yuan, R. Dobbe, *et al*., "Event detection and localization in distribution grids with phasor measurement units," in *Proc. IEEE Power & Energy Society General Meeting*, Chicago, IL, USA, pp. 1-5, 2017.

[11] O. Ardakanian, V. Wong, R. Dobbe, *et al*., "On identification of distribution grids," *IEEE Trans. Control Netw. Syst.*, vol. 6, no. 3, pp. 950-960, Sept. 2019.

[12] F. Si, Y. Han, J. Wang, *et al*., "Connectivity verification in distribution systems using smart meter voltage analytics: A cloud-edge collaboration approach," *IEEE Trans. Ind. Informat.*, vol. 17, no. 6, pp. 3929-3939, June 2021.

[13] W. Zhang, W. Liu, C. Zang, *et al*., "Multiagent system-based integrated solution for topology identification and state estimation," *IEEE Trans. Ind. Informat.*, vol. 13, no. 2, pp. 714-724, April 2017.

[14] J. Peppanen, M. Reno, M. Thakkar, *et al*., "Leveraging AMI data for distribution system model calibration and situational awareness," *IEEE Trans. Smart Grid*, vol. 6, no. 4, pp. 2050-2059, July 2015.

[15] Z. Shi, K. Dong, J. Zhao, *et al*., "An improved statistical algorithm for topology identification and parameter estimation of low-voltage distribution grids," in *Proc. IEEE Sustain. Power and Energy Conf. (iSPEC)*, Chengdu, China, pp. 2500-2505, 2020.

[16] A. Gandluru, S. Poudel and A. Dubey, "Joint estimation of operational topology and outages for unbalanced power distribution systems," *IEEE Trans. Power Syst.*, vol. 35, no. 1, pp. 605-617, Jan. 2020.

[17] J. Zhang, Y. Wang, Y. Weng, *et al*., "Topology identification and line parameter estimation for non-PMU distribution network: A numerical method," *IEEE Trans. Smart Grid*, vol. 11, no. 5, pp. 4440-4453, Sept. 2020.

[18] J. Zhao, L. Li, Z. Xu, *et al*., "Full-scale distribution system topology identification using Markov random field," *IEEE Trans. Smart Grid*, vol. 11, no. 6, pp. 4714-4726, Nov. 2020.

[19] P. Papadopoulos, T. Guo and J. Milanović, "Probabilistic framework for online identification of dynamic behavior of power systems with renewable generation," *IEEE Trans. Power Syst.*, vol. 33, no. 1, pp. 45-54, Jan. 2018.

[20] A. Azizivahed, A. Arefi, S. Ghavidel, *et al*., "Energy management strategy in dynamic distribution network reconfiguration considering renewable energy resources and storage," *IEEE Trans. Sustain. Energy*, vol. 11, no. 2, pp. 662-673, April 2020.

[21] X. He, R. C. Qiu, Q. Ai, *et al*., "A hybrid framework for topology identification of distribution grid with renewables integration," *IEEE Trans. Power Syst*., vol. 36, no. 2, pp. 1493-1503, March 2021.

[22] Z. Tian, W. Wu, *et al*., "A mixed integer quadratic programming model for topology identification in distribution network," *IEEE Trans. Power Syst.*, vol. 31, no. 1, pp. 823-824, Jan. 2016.

[23] H. Zhang, W. Sun, Y. Li, D. Fu and Y. Yuan, "A fast optimal power flow algorithm using power ball method," *IEEE Trans. Ind. Informat.*, vol. 16, no. 11, pp. 6993-7003, Nov. 2020.

[24] S. Boyd, N. Parikh, E. Chu, *et al*., *A Distributed Optimization and Statistical Learning via The Alternating Direction Method of Multipliers*, 1st Edition, Now Publisher Inc., Hanover, USA, 2011.

[25] W. Pan, A. Sootla, and G. Stan, "Distributed reconstruction of nonlinear networks: An ADMM approach," *IFAC Proceedings Volumes*, vol. 47, no. 3, pp. 3208-3213, 2014.

[26] ADRES-Concept, "Autonomous decentralised renewable energy systems,". [Online] Available: https://www.ea.tuwien.ac.at/projects/a-dres_concept/EN/. Accessed on: Feb. 2021.

[27] G. Brauner, D. Tiefgraber, C. Leitinger, *et al*., "ADRES: autonomous decentralized regenerative energy-systems," in *Proc. European PV-Hybrid and Mini-Grid Conference*, Greece, pp. 514-521, May 2008.

[28] R. Nishihara, L. Lessard, B. Recht, *et al*., "A general analysis of the convergence of ADMM," in *Proc. 32nd International Conference on Machine Learning*, vol. 37, pp. 343–352, July 2015.

[29] B. Wahlberg, S. Boyd, M. Annergren, *et al*., "An ADMM algorithm for a class of total variation regularized estimation problems," *IFAC Symposium on Syst. Identification*, vol. 45, no. 16, pp. 83-88, July 2012.

[30] T. Duong, X. Chu, and H. Suraweera, *Ultra-dense Networks for 5G and Beyond Modelling, Analysis, and Applications*, 1st Edition, John Wiley & Sons Ltd., USA, 2019.

[31] B. Li, Y. Chen, W. Wei, *et al*., "Preallocation of electric buses for resilient restoration of distribution network: A data-driven robust stochastic optimization method," *IEEE Systems Journal*, Early Access.

Priyank Shah (Student Member, IEEE) was born in Vadodara, Gujarat, India, in 1992. He received the B.Eng. in electrical engineering from Birla Vishvakarma Mahavidyalaya (BVM), Gujarat, India, in 2013. He joined for M.Tech. degree in power system at the Indian Institute of Technology Delhi in 2015. He received the Ph.D. degree in electrical engineering from the Indian Institute of Technology Delhi, New Delhi, India, in 2020. He is a recipient of convocation award entitled Amit Garg Memorial Research Award from Indian Institute of Technology Delhi and Best Innovative Project Award from Indian National Academy of Engineering (INAE), in November 2020 and December 2020, respectively. He is a recipient of the prestigious POSOCO Power System Award (PPSA) in Doctoral category from Power System Corporation (POSOCO), Gov. of India Enterprise and Foundation for Innovation & Technology Transfer (FITT), IIT Delhi in March 2021. He secured nomination in Top-10 position in 'Energy Solution' category for BRICS Young Scient Award in September 2021. He is also recipient of Second Runner up in ISSS PHD Student Award from Indian Institute of Science (IISc), Bangalore, in 2022.

He is currently working as a Research Fellow at Intelligent Control and Smart Energy Research Group, the University of Warwick. His areas of interest includes synchronization, grid-connected power electronics converter, virtual synchronous generator (VSG), fault ride through operation, leakage current and power quality improvement of the distributed grid.

Xiaowei Zhao received the Ph.D. degree in control theory from Imperial College London, London, U.K., in 2010.

He was a Post-Doctoral Researcher with the University of Oxford, Oxford, U.K., for three years before joining the University of Warwick, Coventry, U.K., in 2013. He is currently Professor of control engineering and an EPSRC Fellow with the School of Engineering, University of Warwick.

His main research areas are control theory and machine learning with applications in offshore renewable energy systems, smart grid, and autonomous systems.